In-Situ Calibration of sPHENIX Hadronic Calorimeter using Isolated Single Hadrons

Emma McLaughlin, Oliver Suranyi, Blair Seidlitz, Bill Zajc

August 18, 2023

Plots I plan to submit for approval are Fig. 2, 3, 5, 6, 7, 11 and 12.

1 Introduction

Fundamental aspects of the nuclear strong force can be studied in the collisions of high energy heavy nuclei, which produce a hot and dense state of deconfined quarks and gluons, known as quark-gluon plasma (QGP). The properties of the QGP can be studied by observing the various particles emerging from the medium, including jets, highly collimated collection of particles created by the fragmentation and hadronization of a high momentum quark or gluon.

An important step in jet reconstruction is the calibration of the jet energy. There are two main approaches to achieve this: the top-down and bottom-up approaches. In case of the top-down approach, both the electromagnetic calorimeter (EMCal) and the hadronic calorimeter (HCal) are calibrated to the electromagnetic scale, then based on Monte Carlo (MC) simulated jets, a jet energy scale correction factor is introduced – this is the default method in sPHENIX. On the other hand, the bottom-up approach achieves the same goal by calibrating the EMCal to the electromagnetic scale and calibrating the HCal to the hadronic scale. Thus the jet energy can be calculated directly from the calorimeter energy deposits.

Measurements of the single hadron E/p distribution can be used to estimate the data and MC differences in calorimeter response [1]; this uncertainty in calorimeter response should be found for both the top-down and bottom-up approaches to jet reconstruction. Therefore, this study can be useful in discerning the uncertainty in calorimeter response between data and MC in the sPHENIX default EM scale calibration. These E/p measurements could also be used to calibrate the sPHENIX HCal to the hadronic scale allowing for sPHENIX to also perform this bottom-up approach to jet reconstruction. In this study, we measure the E/p distribution for isolated single hadrons within Au+Au collisions at $\sqrt{s_{NN}} = 200$ GeV.

For our E/p measurement, we select for isolated hadrons that have a low energy deposition reflective of ionization energy loss in the EMCal. By requiring the isolated hadron have a low energy deposition in the EMCal, we are can use the EMCal to reduce neutral energy in the track isolation cone as well as select for events which begin their showers in the HCal system. We also require HCal cuts of $E_{\mathrm{IHCal},\Delta R=0.1} < 0.1$ GeV and $E_{\mathrm{OHCal}}/p > 0.1$, to further select for these late showering events. Selecting for these events in particular are useful as these distributions will be less susceptible to possibly overlapping EMCal calibration efforts that are currently ongoing.

2 Datasets and Monte Carlo simulations

Data sets were comprised of track, calorimeter cluster and calibrated tower, and MBD (Minimum Bias Detector) North-South-sum centrality measurement information for 10 million Minimum Bias (MB) HIJING Au+Au events from run 7 of the MDC2 data set and truth level and g4hits information for 1 million MB HIJING Au+Au events at $\sqrt{s_{NN}} = 200$ GeV from run 7 of the MDC2 data set. This data was generated using:

```
CreateFileList.pl -type 4 -run 7 DST_TRACKS DST_TRUTH DST_CALO_CLUSTER
DST_BBC_G4HIT DST_TRKR_CLUSTER DST_TRKR_G4HIT
```

Additionally, 100,000 single particle events were generated using π^- with a flat p_{T} range of $[0.5, 4]$ GeV. Truth, track, calorimeter cluster/tower and g4hit information was generated for this data as well. In all data sets, tracks are projected to the front and back faces of each calorimeter layers using the corresponding module of ACTs. The projected η and ϕ values of the tracks to a given calorimeter layer are calculated as the average from the corresponding front and back face values.

3 Event selection and track isolation

We first apply a conservative event centrality cut of centrality $> 20\%$ to the MB HIJING data to exclude the most central collisions where track isolation is highly unlikely.

We then select for tracks with $|p_{\mathrm{T}}| > 1.0$ GeV and $|\eta| < 1.0$ as Single Hadron candidates (SH). These tracks are checked for isolation by requiring that there is no other track projected in the $\Delta R = 0.4$ cone around the track projection point.

For this isolation, the track projection to the center of the EMCal is used as the track's (η, ϕ) location when available. For very low momentum tracks, the tracks' projection to the front face of the EMCal may be used if the projection to the back face of the EMCal was not found by the projection algorithm. The isolated SH candidates are also required to have a projection to the EMCal front face. This cut eliminates less than 0.05% of the track candidates that fulfill the kinematic and isolation requirements.

Tracks that fulfill the above kinematic and isolation requirements are also required to fulfill the following track quality criteria:

- the event should have a valid primary vertex with $|v_z| < 10$ cm,
- the track fit should have $\chi^2/\mathrm{ndf} < 10$,
- number of hits in the MVTX be greater or equal to 2,
- number of hits in the INTT be greater or equal to 1,
- number of hits in the TPC be greater or equal to 24

More information on the application of these default tracking cuts to this study can be found in Section A of the Appendix.

In the case of isolation on the track-level, all tracks in the event were used to find the isolation radius around a given track. To isolate on truth-level (which we use to ascertain the effect of neutral neighboring particles in the collision which do not show up in the tracking information), we use the truth information from Geant4. Specifically, we consider neutral, primary particles with momentum larger than 0.2 GeV when looking for neutral energy isolated tracks. We found that less than 1% of particles with momentum smaller than 0.2 GeV make it to the EMCal.

Once a track passes the required kinematic, isolation, quality (and possibly neutral energy isolation) criteria, calorimeter towers from each calorimeter within $\Delta R = 0.2$ of the track projection to each calorimeter are matched to the track.

3.1 Track projection performance

To correctly match the showers of energy in calorimeter towers to isolated tracks, we first investigated whether it was sufficient to use the tracks' projections to the towers' front-face only. Here, we looked at the distribution of $\delta\eta = \eta_{\mathrm{trk}} - \eta_{\mathrm{g4hit}}$ and $\delta\phi = \phi_{\mathrm{trk}} - \phi_{\mathrm{g4hit}}$, where η_{trk} is the track projection η value to the calorimeter. The $\delta\eta$ and $\delta\phi$ distributions for the track projection to the front face versus center of the calorimeter are shown in Fig. 1.

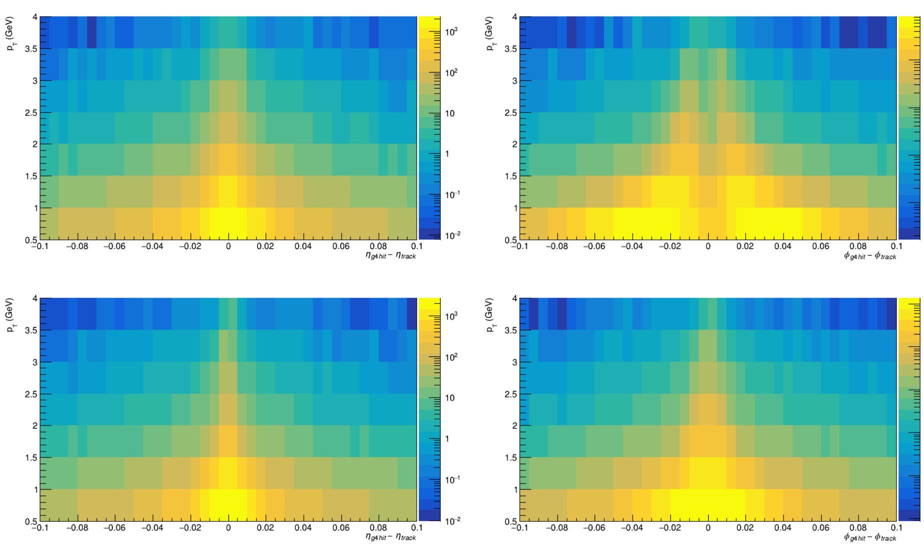

Figure 1: $\delta\eta$ (left) and $\delta\phi$ (right) distributions for the track projection to the front face of the EMCal (top plots) and the track projection to the center of the EMCal (bottom plots).

When calorimeters are projected to the front faces of the calorimeter, the estimated position of the shower will be biased as particles arrive at an angle to the surface of the detector and the center-of-gravity of the particle's energy deposition will be shifted by a given amount. This arrival angle is in part due to the particle's interaction with the magnetic field in the detector, hence the angle depends on the charge of the particle and the $\delta\phi$ distribution to the front of the EMCal in Fig. 1 is bimodal. Furthermore, the effect is more pronounced at low p_{T}, where the tracks are more curved, thus arriving at a larger angle with respect to the calorimeter surface.

We see this bimodal distribution for track projections to the front face of the EMCal for particles with p_T up to 4 GeV/c. When projecting tracks to the center of the EMCal, we find that the $\delta\phi$ distribution is now centered at zero and there is no longer a bimodal ϕ shift in the $\delta\phi$ distribution based on particle charge, giving a much better matching between the track location and the location of calorimeter energy deposition. Therefore, for all track-calorimeter tower matching done in this study, we use the track projections to the center of all three of the calorimeters (EMCal, IHCal and OHCal).

3.2 Track rates

Following the previously outlined set of tracking cuts, we report the rate of good tracks for centrality bins of $20-40\%$, $40-60\%$, $60-80\%$ and $80-100\%$ in Fig 2. The major limiting factor for getting high statistics for this study is the $\Delta R = 0.4$ isolation cut applied to all good tracks. We find that events in centrality bin $60-80\%$, have the greatest yield of good tracks with 0.25 tracks per event. Events in both centrality bins $40-60\%$ and $80-100\%$ have a yield of 0.13 tracks per event, a factor of 2 lower than in the $60-80\%$ centrality bin, and the most central events looked at in this study have a yield of 0.01 tracks per event, a factor of 10 lower than any other centrality bin looked at in this study. This study uses the current suggested default tracking cuts (excluding the DCA cut). However, further investigation into the tracking quality with slight alterations to these cuts should be studied in the future to see if we can increase the rate of good tracks without compromising track quality.

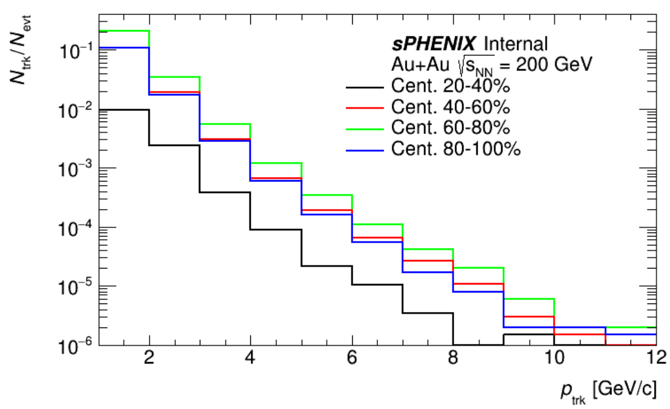

Figure 2: Rate of good tracks per event with a track isolation radius of $\Delta R = 0.4$ in HIJING Au+Au $\sqrt{s_{NN}} = 200$ GeV events.

4 Calorimeter shower sizes

To determine the best radius to use for our track-calorimeter tower matching, we studied the single hadron shower size via multiple methods. We first used our π^- particle gun data set to determine the fraction of total energy in cones of radius $\Delta R = 0.1, 0.2$ and 0.3, where $\Delta R = \sqrt{\Delta\eta^2 + \Delta\phi^2}$. The energy deposition within a cone of ΔR is comprised of all calorimeter towers within ΔR of the track projection. Using the method described in the next section for truth classifying shower start locations in the calorimeter systems, we select for particle gun events with OHCal showers and show the fraction of total energy in cones of radius $\Delta R = 0.1, 0.2$ and 0.3 in all calorimeters for these events in Fig. 3. Here, we can see that a shower size of $\Delta R = 0.2$ is most suitable with a mean fraction of energy in the $\Delta R = 0.2$ cone of 96%. The mean fraction of energy in the $\Delta R = 0.3$ at 98% only has marginal benefits over the $\Delta R = 0.2$ and would require a larger track isolation cone which would significantly decrease the rate of good tracks in Au+Au MB data.

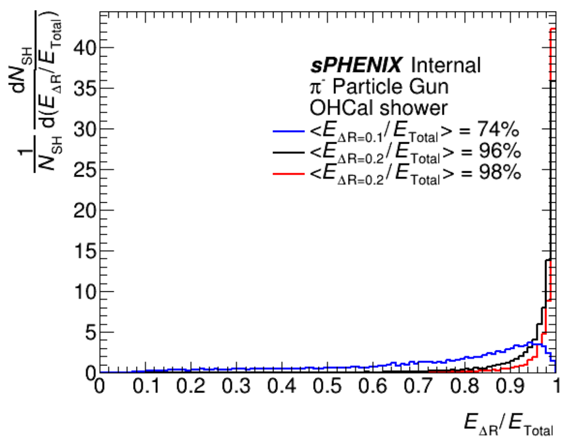

Figure 3: Fraction of EMCal + IHCal + OHCal energy within cone of $\Delta R = 0.1$ (blue), $\Delta R = 0.2$ (black) and $\Delta R = 0.3$ (red) for π^- particle gun OHCal shower events.

In our second method of determining the shower size, we estimated the transverse size of the showers using the weighted sample standard deviation:

$$\sigma_\eta = \sqrt{\frac{\sum_i E_i(\eta_i - \bar{\eta})^2}{\sum_i E_i}} \qquad \sigma_\phi = \sqrt{\frac{\sum_i E_i(\phi_i - \bar{\phi})^2}{\sum_i E_i}} \tag{1}$$

We determined the σ_η and σ_ϕ distributions using both calorimeter tower and g4hits using the π^- particle gun data set. These distributions are shown in Fig. 4.

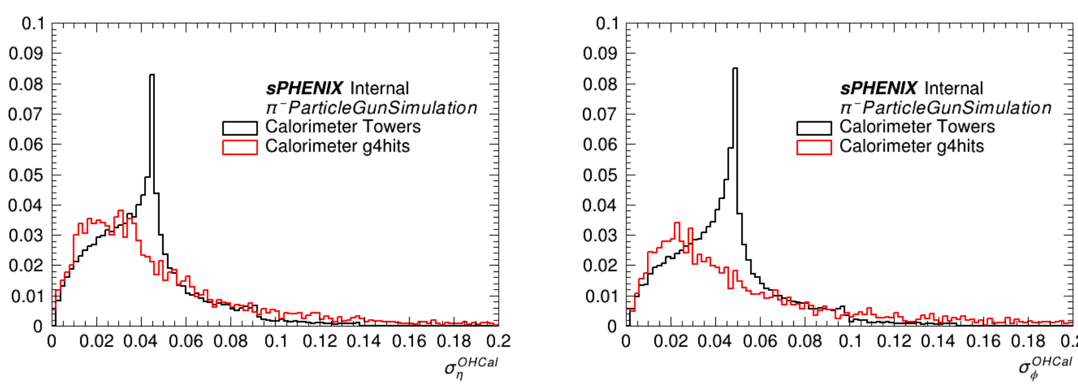

Figure 4: OHCal shower distribution energy weighted widths in η (left) and ϕ (right) for flat p_T distribution π^- particle gun using both calorimeter towers and g4hits.

We find that for both of these methods of calculating the shower width, σ_η and σ_ϕ values of about 0.1 encapsulate nearly all of the distribution, with the majority of the distribution within σ_η and σ_ϕ values of 0.07. Therefore, taking a 2σ width for both our η and ϕ distributions, we find good agreement with the previous method for selecting a shower size of $\Delta R = 0.2$. Additionally, the peak structure found in the calorimeter tower σ_η and σ_ϕ distributions is due to aliasing from the finite size of the HCal towers, which have size $\delta\eta = 0.1$ and $\delta\phi = 0.1$. This peak structure goes away and the distribution gets tighter for the calorimeter g4hit σ_η and σ_ϕ which uses the precise η and ϕ location of each g4hit.

5 Selection of HCal showers

In order to measure E/p for isolated single hadrons showering in the HCal, we first need an understanding of how to select for low-energy or Minimum Ionizing Particle (MIP)-like energy deposition in the EMCal.

5.1 Truth level classification of shower location

We first define a method for finding where in the detector the hadron begins showering on a truth-level using the truth particle and vertex information from Geant4. An isolated single hadron is considered to have begun showering at the first truth information vertex containing more than one daughter particle that is not an electron or photon. This method for selecting MIP-like particles at the truth level, correctly classified 99.99% of particles which MIP through the entire detector and were found in the blackhole volume outside of the full detector volume. Additionally, isolated hadrons that undergo known weak decays including $\pi^{+/-} \rightarrow \mu^{+/-} + \nu_\mu$ were not included as possible events as the daughter particles should MIP through the remainder of the detector and therefore do not constitute late showering events.

Shower Start	p = 0-1 GeV/c	1-2 GeV/c	2-3 GeV/c	3-4 GeV/c	4-5 GeV/c
Tracker	1	2	1	3	2
EMCal	59	60	60	58	63
IHCal	10	10	10	9	7
Magnet	6	7	8	8	7
OHCal	7	12	17	18	19
Only EM deposit	16	9	4	4	1

Table 1: Rates (%) for given momentum bin of isolated hadrons beginning a shower in selected detector based on truth particle vertex information. Weak decays included in Only EM deposit category.

Using our method, we can now classify isolated single hadron events based on where their shower begins at the truth level. The rates of shower start location for our 100,000 π^- single particle dataset with a flat p_T range of $[0.5, 4]$ GeV/c are included in Table 5.1. For all momentum bins the majority of isolated hadrons begin showering in the EMCal. Additionally, nearly all (>90%) of the tracker shower events are started by an interaction with the TPC outer field cage.

5.2 Low energy/MIP-like deposition in EMCal

To find the optimal energy and radius cuts for selecting late showering hadrons with low energy deposition in the EMCal, we used truth information about the showering vertex history of these isolated hadrons. We studied a range of magnitudes and radii (ΔR) for EMCal energy deposition, to identify the optimal pair based on the purity and efficiency of the truth MIP-like deposition, where:

$$\text{Purity} = \frac{N_{\text{true MIP+MIP selection}}}{N_{\text{MIP selection}}} \qquad \text{Efficiency} = \frac{N_{\text{true MIP+MIP selection}}}{N_{\text{true MIP}}} \tag{2}$$

The results of these purity and efficiency studies are shown in Fig. 5.

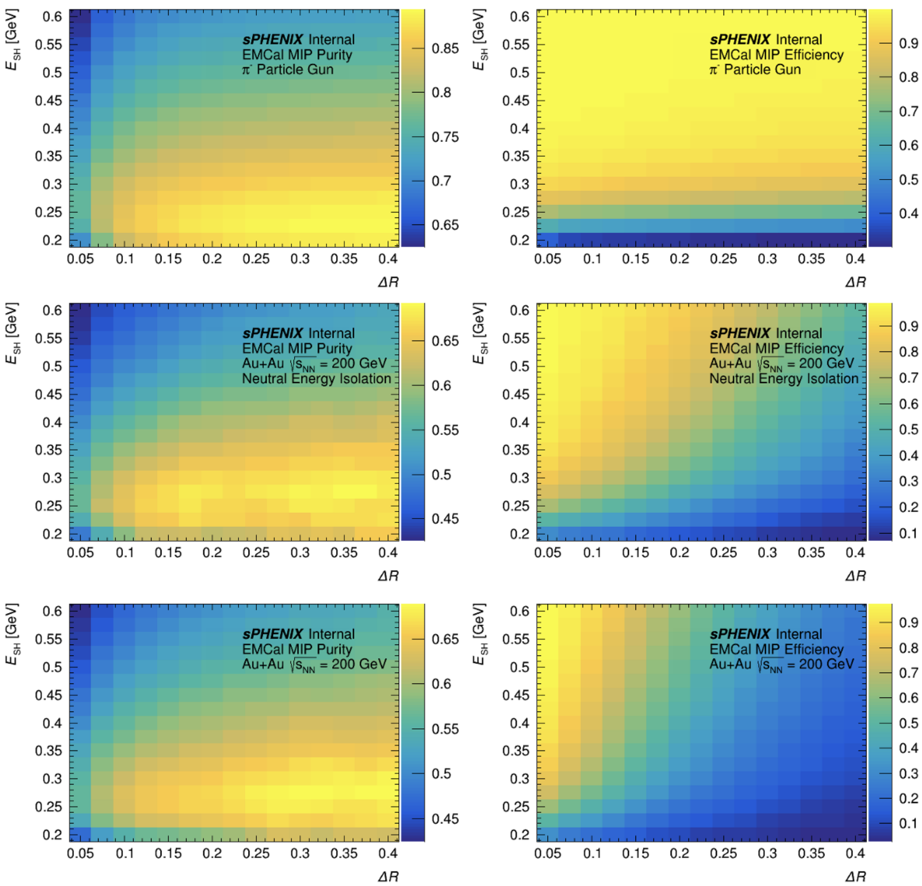

Figure 5: EMCal MIP purity (left) and efficiency (right) for various ΔR and Energy deposition values in particle gun simulation (top), truth isolated hadrons in MB HIJING (center) and isolated hadrons in MB HIJING (bottom).

We can see from Fig. 5, the effect of both a falling particle energy spectra and additional neighboring particles in MB HIJING on the MIP purity and efficiency. First, we see the MIP efficiency is independent of the ΔR value in the flat p_T particle gun dataset, while we see a very strong anti-correlation between MIP efficiency and ΔR value in the MB HIJING data set. The efficiency at large ΔR is somewhat better for the MB HIJING isolated single hadron events that also pass a neutral energy isolation cut, meaning they do not have any neutral particles in their track isolation cone determined by truth information, but as we approach the isolation radius of $\Delta R = 0.4$, the efficiency in these cases drops as well as energy from particles outside of the isolation cone that have started to shower creeps into the isolation cone. Further, we can see in from the MIP purity rates that the falling particle energy spectrum in MB HIJING results in an overall lower purity rate as the shower energy distribution overlaps more with the MIP energy distribution than in the particle gun case with a flat p_T distribution. From these studies, values of $\Delta R = 0.1$ and E = 0.35 GeV were selected as the best option for optimizing the purity and efficiency of truth MIP-like energy deposition in the EMCal for the MB HIJING sample with a purity of 60% and an efficiency of 72%. The energy profiles for EMCal truth MIP and truth shower isolated single particles for a calorimeter area of $\Delta R = 0.1$ are shown in Fig. 6. From Fig. 6, we can see that a good delineation of MIP and shower energy deposition is at E = 0.35 GeV.

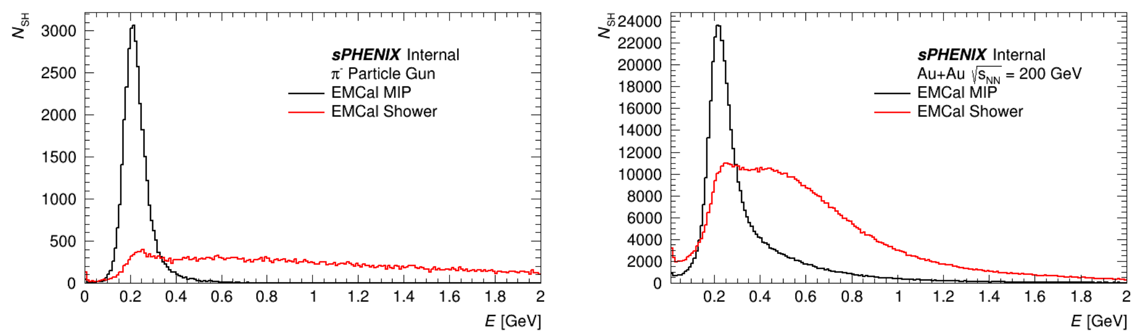

Figure 6: EMCal truth MIP and shower energy deposition for $\Delta R = 0.1$ tower range in particle gun simulation (left) and isolated hadrons in MB HIJING (right).

The distributions have a higher level of overlap for the isolated single hadrons in the MB HIJING dataset than in the particle gun dataset for two reasons. The first reason is because of the falling spectrum of particle energy in the MB HIJING dataset which has a higher rate of low energy particles showering than in the flat p_T particle gun dataset resulting in the shower energy distribution being greater at low energies closer to the EMCal MIP peak. The second reason is because of the addition of neutral energy which cannot be isolated against in the $\Delta R = 0.1$ cone of EMCal towers which causes the MIP energy distribution to have a longer tail in the MB HIJING dataset moving the MIP distribution more towards the shower distribution.

6 Measurement of E/p distributions

6.1 Full E/p distribution

We report in Fig. 7 the full E/p distribution for all isolated single hadrons without any cuts to the calorimeter energy applied. We calculate the E/p distribution for each of our isolated good tracks by summing the energy deposition in the matched towers in all three calorimeters and dividing by the particle momentum.

In Fig. 8, we can see the full E/p distribution from Fig. 7 overlaid with the E/p distributions from each of the truth classified shower start detector locations. We can see that for this E/p distribution, a majority of the isolated SH events begin in the EMCal. An important note here is that a shower can begin at the end of the EMCal volume, for example, deposit little energy into the EMCal and continue into the IHCal, Magnet and OHCal detector volumes to deposit the remainder and majority of their energy. This SH event would still be classified as a shower event that began in the EMCal. Therefore, the shower start classification can

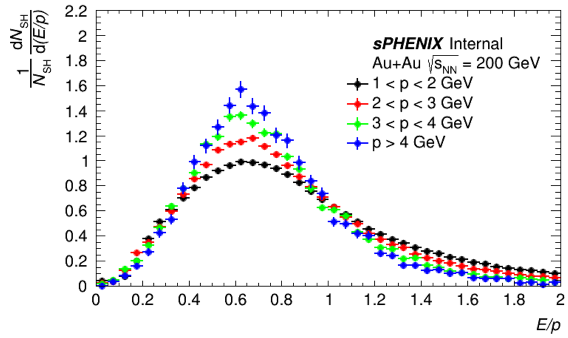

Figure 7: Full E/p distribution for isolated single hadrons in MB HIJING.

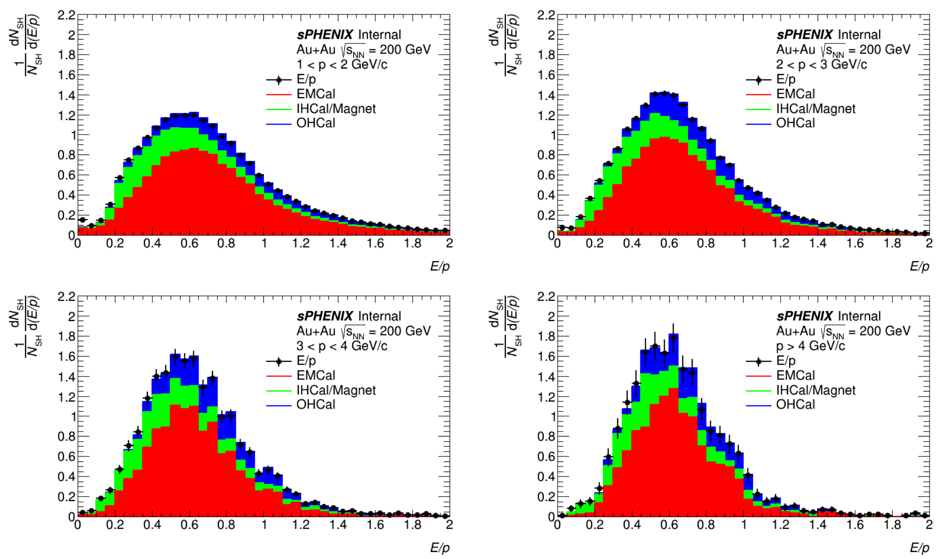

Figure 8: Full E/p distributions for isolated single hadrons in MB HIJING overlaid with E/p distributions for SH classified by the location of their shower start.

be misleading in the ratio of energy deposition in the calorimeters. However, for this study, classifying by shower start location is ideal for isolating for events that only deposit shower energy in the HCal detectors.

6.2 Selecting for late showering hadrons with EMCal MIP cut

The E/p measurement for isolated single hadrons from our 10 million event MB HIJING data set with which pass our EMCal MIP cut is shown in Fig. 9.

From Fig. 9, we can see a two peaked shape to the E/p distribution at low momentum ($p < 2$ GeV/c) that goes away at higher momentum ($p > 3$ GeV/c). To investigate this double peaked shape, we once again classified all isolated tracks which pass our EMCal MIP cut using our 1 million MB HIJING dataset with truth information and overlap our E/p distribution from the 10 million MB HIJING dataset with these classified E/p distributions.

Fig. 10 shows the E/p distributions from Fig. 9 overlapped with these truth-classified E/p distributions. We can see clearly in the $1 < p < 2$ GeV/c and $2 < p < 3$ GeV/c E/p

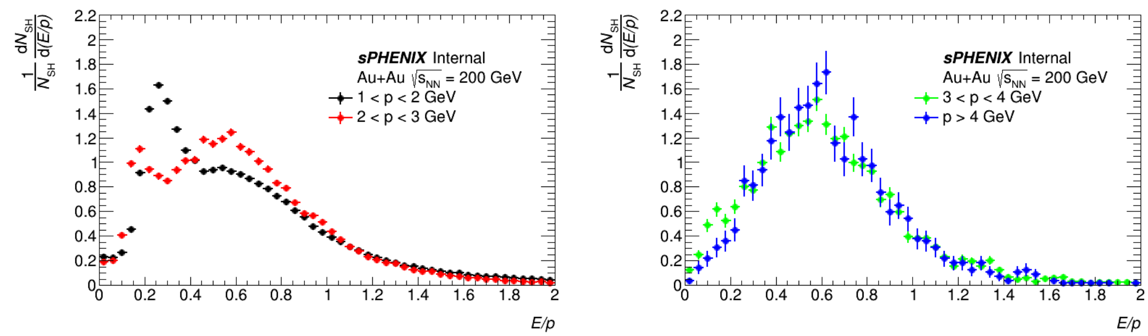

Figure 9: E/p distributions isolated single hadrons which pass the EMCal MIP energy cut, $E_{\mathrm{EMCal},\Delta R=0.1} < 0.35$ GeV, and no HCal cut from MB HIJING for $1 < p < 3$ GeV/c (left) and $p > 3$ GeV/c (right).

distributions that this double peaked structure arises from the different energy distributions for showers that begin before the magnet, showers that begin in the EMCal, IHCal, or in the magnet and showers that begin after the magnet, namely showers in the OHCal. Additionally, for the $1 < p < 2$ GeV/c momentum bin, we see that a substantial fraction, 22%, of the E/p distribution is coming from EMCal showers which pass the EMCal MIP criteria. This fraction in the lowest momentum bin of our distribution is especially concerning because of the steeply falling spectrum of track multiplicity with momentum in MB Au+Au events which results in the majority of our good isolated single hadrons falling into this lowest momentum bin for our in-situ study.

6.3 Selecting for late showering hadrons using HCal cuts

In a similar method to [1] to select for late showering single hadrons, or showers beginning in the OHCal, we employ an energy cut requirement on E_{OHCal}/p and a MIP-like cut on the IHCal. We apply a cut of $E_{\mathrm{OHCal}}/p > 0.1$ and $E_{\mathrm{IHCal},\Delta R=0.1} < 0.1$ GeV for all isolated single hadrons which also pass the EMCal MIP cut. The resulting full E/p distributions with truth-classified overlays are shown in Fig. 11. With this cut applied, we no longer see the double peaked structure in the E/p distribution for low momentum bins, and the fraction of EMCal showers which pass both cuts and are included in the E/p distribution decreases to 10% for the lowest momentum bin and 3% for the highest momentum bin.

Using both the EMCal MIP cut and the late-showing HCal cuts, we are able to isolate E/p distributions for isolated single hadrons showering in the HCal with 90-97% purity. These E/p distributions, shown in full in Fig. 12 (left) and with peak and standard deviation values reported in Fig. 12 (right, bottom), can be used to complete this study's first goal of comparison between Monte Carlo simulation and data to look at the calorimeter response differences of sPHENIX's HCal with its current calibration at the electromagnetic scale as we are able to isolate the HCal response here with minimum EMCal input to the E/p distribution.

When comparing Figs. 10 and 11, we can see that while the EMCal fraction of the selected events decreases, the E/p distribution for all shower location classifications is shifted to higher energies by this $E/p_{\mathrm{OHCal}} > 0.1$ cut. Therefore, we argue that the full E/p distribution would be better to use for the long term goal of calibrating the OHCal to the hadronic scale. Instead within these distributions, the underlying distributions of EMCal/IHCal/Magnet showers

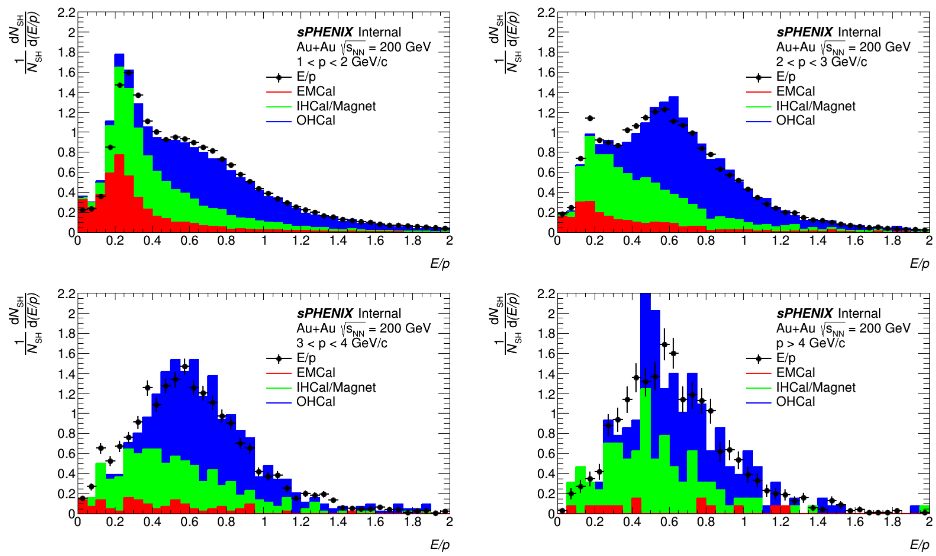

Figure 10: E/p distributions isolated single hadrons which pass the EMCal MIP energy cut, $E_{\mathrm{EMCal},\Delta R=0.1} < 0.35$ GeV, and no HCal cut from MB HIJING overlaid with E/p distributions for SH classified by the location of their shower start.

versus fully OHCal showers should be further investigated to extract the OHCal shower part of these total E/p distributions. A more complete picture of the effect of this E_{OHCal}/p cut on the overall E/p can be found in Section B of the Appendix.

7 Conclusion

In this study, we outline a method for using the E/p measurements from isolated single hadrons to estimate the uncertainty in the calorimeter response to single hadrons between Monte Carlo simulation and data as well as calibrate the sPHENIX HCal to the hadronic scale. The E/p measurement in this study has been completed using only tracks and calorimeter tower information from MB HIJING, allowing for direct comparison to and in situ calibration using Au+Au data. We report for isolated single hadrons with $1 < p < 2$ GeV/c, a peak value of E/p of 0.555, for $2 < p < 3$ GeV, a peak value of E/p of 0.552, for particles with $3 < p < 4$ GeV, a peak value of E/p of 0.573, and particles with $p > 4$ GeV, a peak value of E/p of 0.558. These E/p values can be very useful in their comparison to sPHENIX Au+Au data, both as a method of discerning the data and MC differences in the hadronic calorimeters' responses at the EM scale and as a possible absolute calibration of HCal to the hadronic scale.

References

[1] G. Aad et. al. Single hadron response measurement and calorimeter jet energy scale uncertainty with the ATLAS detector at the LHC. *The European Physical Journal C*, 73(3), mar 2013.

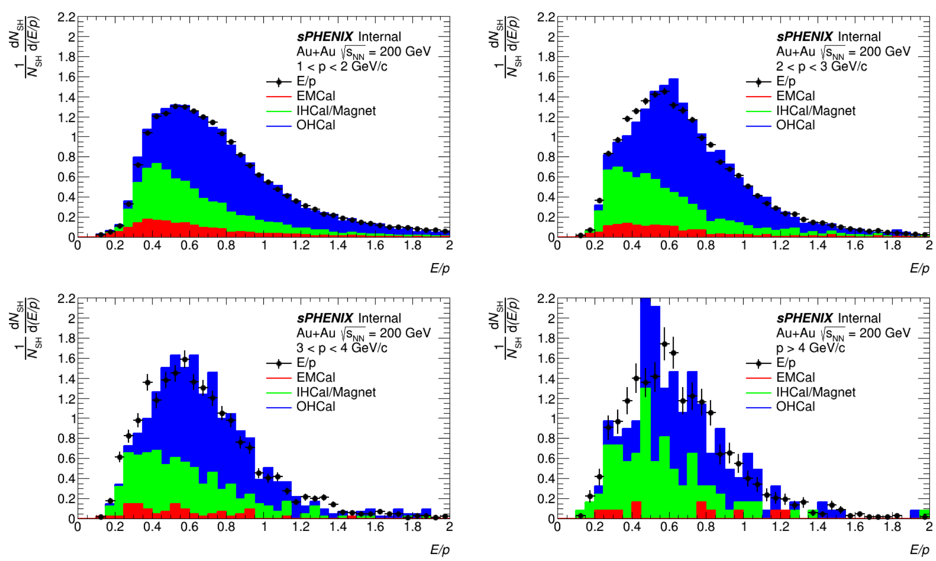

Figure 11: E/p distributions isolated single hadrons which pass the EMCal MIP energy cut, $E_{\text{EMCal},\Delta R=0.1} < 0.35$ GeV, and HCal late-showering cuts, $E_{\text{IHCal},\Delta R=0.1} < 0.1$ GeV and $E_{\text{OHCal}}/p > 0.1$ GeV, from MB HIJING overlaid with E/p distributions for SH classified by the location of their shower start.

A Using sPHENIX Nominal Tracking Cuts

A.1 Primary vertex properties

The position distributions of the primary vertices (PV) is shown in Fig. 13. It can be seen that the PVs for this MB HIJING data set are spread along the z-axis from -10 cm to 10 cm and are relatively close to the beamline. The spread in the X_{PV} and Y_{PV} should be due to intrinsic tracking resolution when reconstructing the primary vertex as the primary vertex from HIJING for these runs has $X_{PV} = 0$ and $Y_{PV} = 0$.

Furthermore, a lot of events are found with exactly $(0, 0, 0)$ primary vertex position. This is the artifact of the software: when no primary vertex is found, still a vertex in $(0, 0, 0)$ is stored in the event. Therefore, when requiring the primary vertex be valid, we require that the vertex not be (0,0,0). The events affected by this cut have a small number of tracks (< 5). This is demonstrated in Fig. 13.

This primary vertex cut did not heavily influence our isolated single hadron sample, 0.02% of isolated SH which passed the kinematic and isolated criteria did not pass this cut.

A.2 Track quality distributions

In this section, all quantities are studied for tracks passing the isolation and kinematic criteria. The track quality (χ^2/ndf) distribution is shown in Fig. 14. It can be seen that majority of the tracks fulfills the $\chi^2/\text{ndf} < 10$ criterion. The distributions of the 3-dimensional DCA is shown in Fig. 15. This shows, that the originally suggested 0.002 cm (20 μm) cut on the DCA values is too tight and would result in the loss of the majority of the good tracks. For the rest of this present study, we do not include a DCA cut, but this can be amended in the future when tracking cut suggestions are updated.

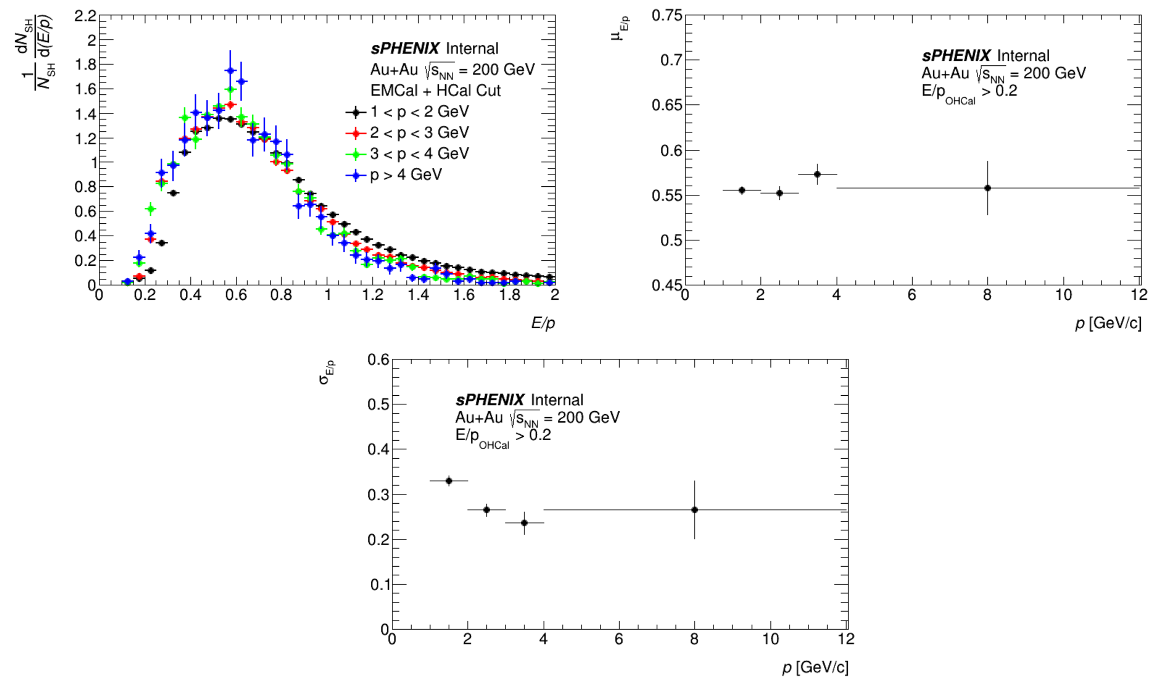

Figure 12: E/p distributions isolated single hadrons which pass the EMCal MIP energy cut, $E_{\mathrm{EMCal},\Delta R=0.1} < 0.35$ GeV, and HCal late-showering cuts, $E_{\mathrm{IHCal},\Delta R=0.1} < 0.1$ GeV and $E_{\mathrm{OHCal}}/p > 0.1$ GeV, from MB HIJING. The peak and standard deviation values for the distributions were calculated by fitting the distributions to a gaussian function in the region surrounding the peak ($E/p = 0.4$ to $E/p = 0.8$).

The number of hits in each tracker system, the MAPS-based VerTeX Detector (MVTX), the Intermediate Silicon Tracker (INTT) and Time Projection Chamber (TPC), are also used as track quality cuts. Distributions for the hits in each of these tracking detectors are shown in Fig. 16 for tracks that have already passed the isolation and kinematic criteria. We see that a majority of the tracks pass all three tracker hit requirements. However, these three tracker hit cuts do reject a combined 38% of isolated single hadron candidates which pass the above cuts.

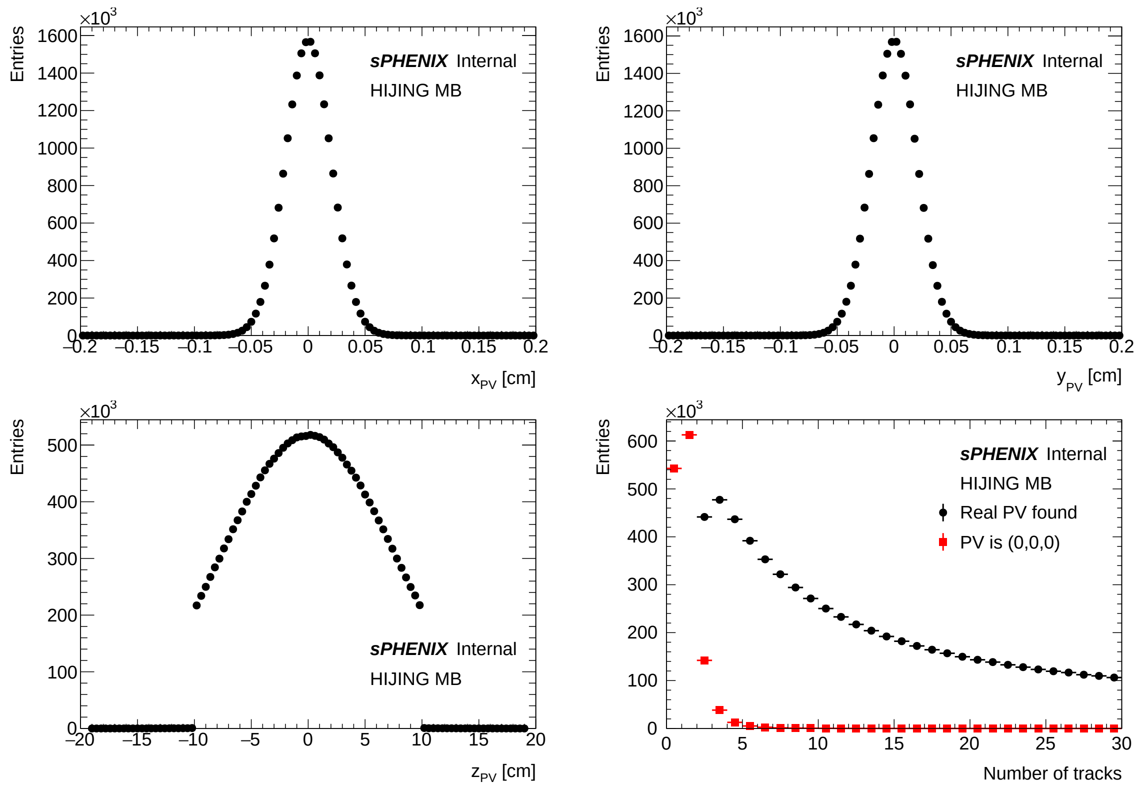

Figure 13: The distribution of primary vertex x (top left), y (top right), and z-coordinates (bottom left). The number of tracks in events with (black) and without (red) a valid primary vertex (bottom right). When no primary vertex is found, a primary vertex with coordinates $(0, 0, 0)$ still saved by the software.

B E/p distribution for Various HCal Cuts

We looked at multiple different E_{OHCal}/p ratios, when looking to apply a late-showering HCal cut to the isolated SH events. We considered E_{OHCal}/p ratios of 0.1, 0.2, 0.3 and 0.4. The E/p distributions for events with E_{OHCal}/p ¿ 0.1 are shown in Fig. 11. Below are the E/p distributions for each of these remaining cases with the truth classified shower start E/p distributions overlaid to highlight the contributions from each of the sPHENIX calorimeters.

We can see that really beyond the first cut applied of E_{OHCal}/p ¿ 0.1, the fraction of EMCal showers does not drastically change and the E_{OHCal}/p cut begins to bias the full E/p distribution, shifting the E/p mean towards higher values of E/p.

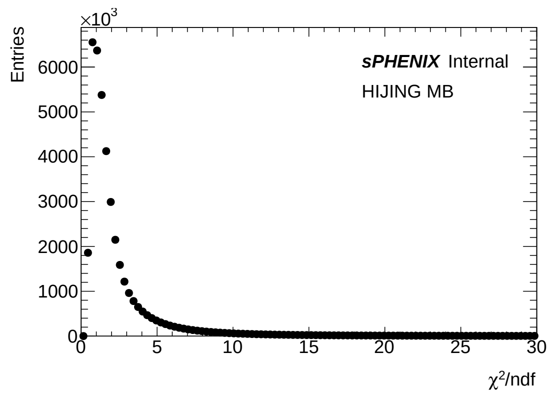

Figure 14: The χ^2/ndf value of track fits.

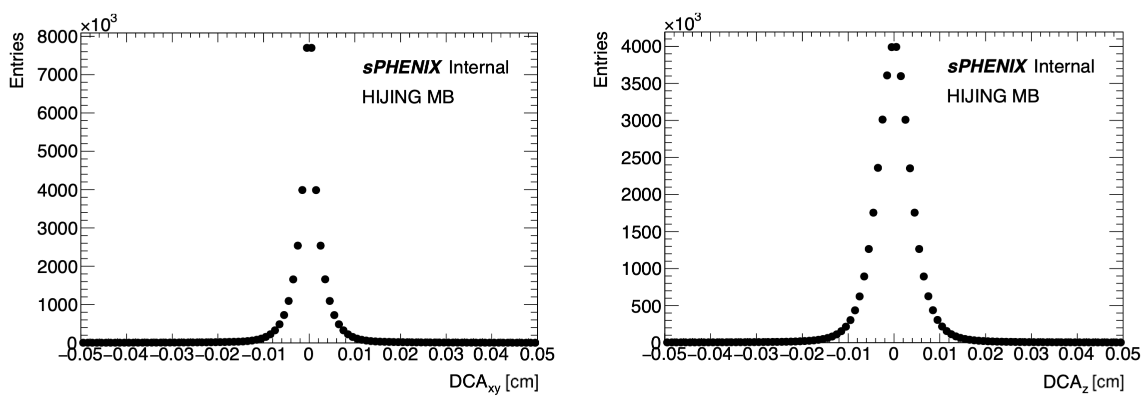

Figure 15: The distribution of the DCA in the x–y-plane (left) and and from the z-coordinate of the PV (right).

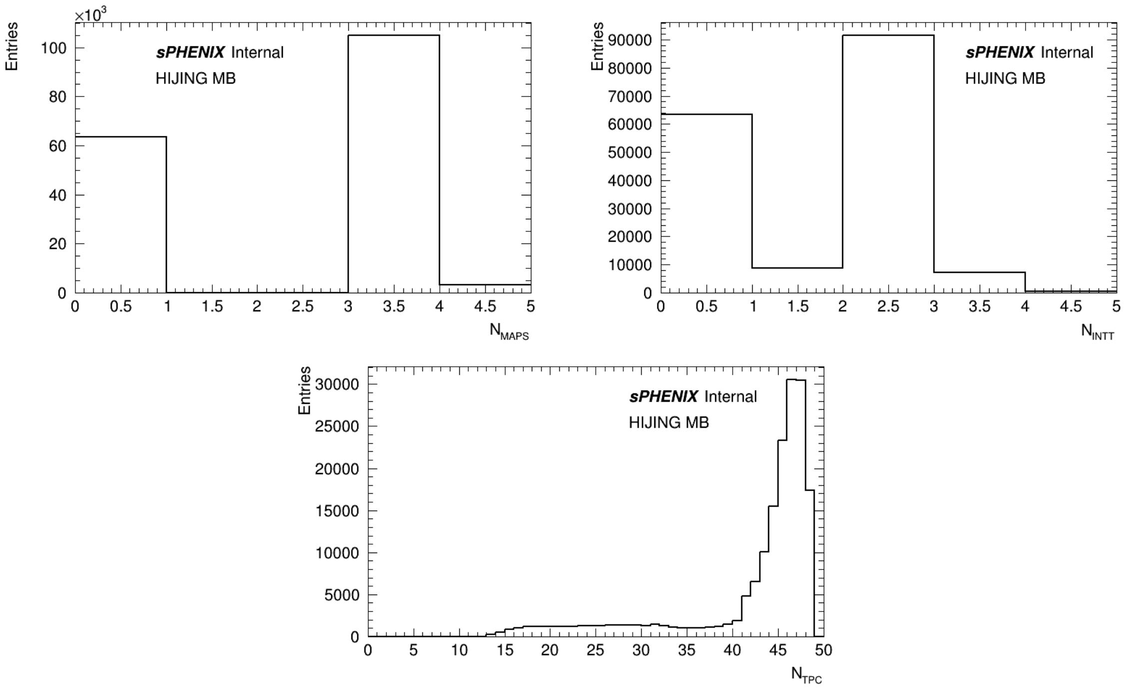

Figure 16: The distribution of tracker hits for the three sPHENIX tracking detectors, MVTX (upper left), INTT (upper right) and TPC (lower).

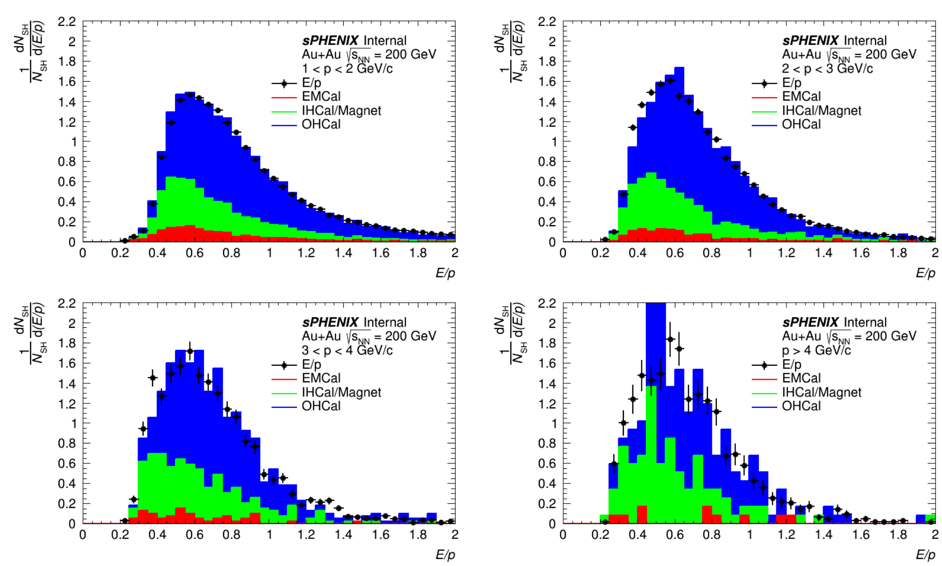

Figure 17: E/p distributions isolated single hadrons which pass the EMCal MIP energy cut, $E_{\mathrm{EMCal},\Delta R=0.1} < 0.35$ GeV, and HCal late-showering cuts, $E_{\mathrm{IHCal},\Delta R=0.1} < 0.1$ GeV and $E_{\mathrm{OHCal}}/p > 0.2$ GeV, from MB HIJING overlaid with E/p distributions for SH classified by the location of their shower start.

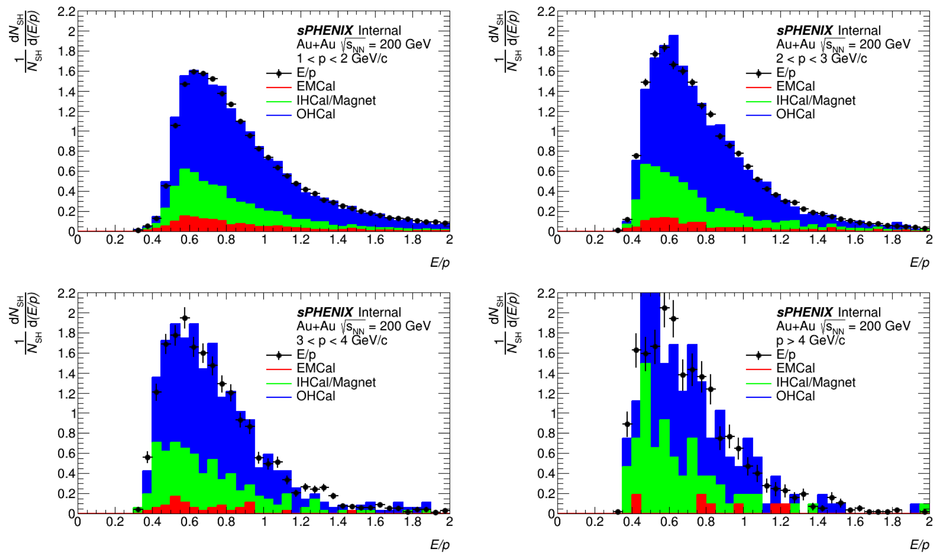

Figure 18: E/p distributions isolated single hadrons which pass the EMCal MIP energy cut, $E_{\mathrm{EMCal},\Delta R=0.1} < 0.35$ GeV, and HCal late-showering cuts, $E_{\mathrm{IHCal},\Delta R=0.1} < 0.1$ GeV and $E_{\mathrm{OHCal}}/p > 0.3$ GeV, from MB HIJING overlaid with E/p distributions for SH classified by the location of their shower start.

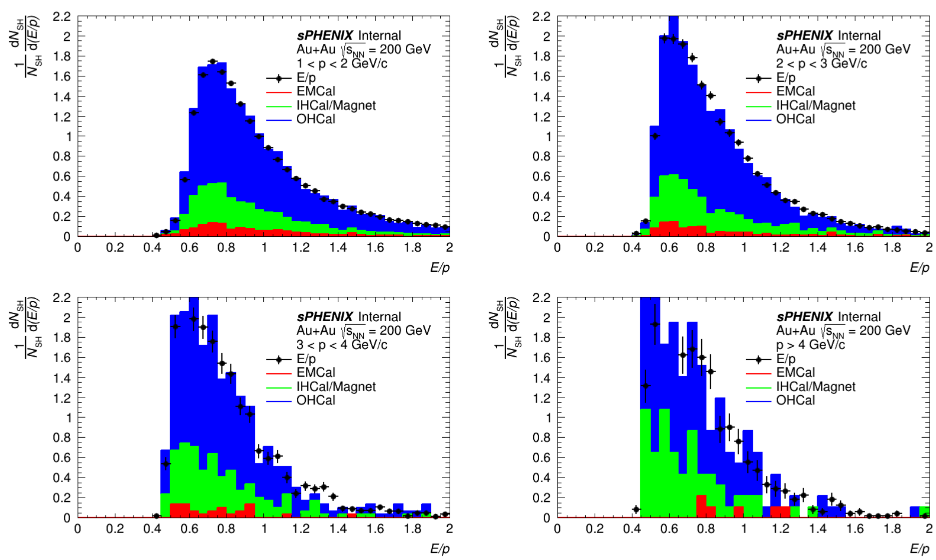

Figure 19: E/p distributions isolated single hadrons which pass the EMCal MIP energy cut, $E_{\mathrm{EMCal},\Delta R=0.1} < 0.35$ GeV, and HCal late-showering cuts, $E_{\mathrm{IHCal},\Delta R=0.1} < 0.1$ GeV and $E_{\mathrm{OHCal}}/p > 0.4$ GeV, from MB HIJING overlaid with E/p distributions for SH classified by the location of their shower start.